Instrumentation of an Inspection Test Rig for Geometry Measurement of Fiber Bundles in Automated Composite Manufacturing

Stefan Neunkirchen, Ewald Fauster, Sophia Lehner and Paul O'Leary

***Abstract*—The major advantage of products made from composite materials is given by their superior weight-specific mechanical properties. These can be weakened by defects induced in the manufacturing process. Therefore, online detection and analysis of the processed fiber bundle geometry is a key factor for the quality assurance of the final part. In this paper, the instrumentation and data evaluation for determining the surface geometry of fiber bundles by means of light sectioning was examined. Bundles of glass and carbon fibers were measured continuously on an inspection test rig. Different background materials have been used in order to validate the applicability of the approach. By utilization of a polynomial fitting algorithm, data segmentation of object and baseline was robustly achieved. By means of cross-correlation, the data alignment could be evaluated faster and more reliable compared to a method previously presented by the authors. The information could then be used for the determination of the fiber bundle width, centerline, spatial changes, and oscillations. In addition, unwanted defects as well as lateral movement of the fiber bundles were reliably detected. The information revealed by the proposed algorithm provides the basis for robust online monitoring of fiber bundle geometry in highly automated composite manufacturing processes.**

***Index Terms*—Discrete fourier transforms, geometry, laser measurement applications, manufacturing data processing, optical position measurement, optical signal processing**

I. Introduction

MONITORING material parameters plays a key role in automated composite manufacturing processes. To provide a more general approach on the instrumentation and the measurement of rovings[1] in automated filament winding processes, this paper is an extension of the I2MTC conference contribution [1]. Therefore, new experiments on the roving inspection test rig were executed with three different fiber types on four varying backgrounds. This provides a more extensive view on the required instrumentation and its limits. Additionally, the algorithm for data structuring and evaluation was improved to provide a more robust evaluation of the processed data. The overall objective stays the same: To measure and detect unintended behavior of the roving in the continuous filament winding process, such that the quality and yield of the plant can be improved.

For high-performance parts, especially in the aerospace industry, processing of continuous rovings is of high relevance. The processes of automated tape laying (ATL), filament winding and automated fiber placement (AFP) have been automated for high-volume production [2]. A good overview of image-based inspection techniques for (wet) filament winding is given in [3]. However, the in-line realtime inspection and quality control has not kept pace with the automation of the processes. In many cases, manual visual inspection is still mandatory. This has lead to a variability in quality and a low yield for aerospace components. Sometimes manual inspection even takes longer than the actual production process [2], [4]. The low yield and high costs of manual inspection emphasise the need and importance for the development of in-line realtime inspection during the manufacturing process.

Up to now, there is no standard method for the automated inspection of carbon fiber reinforced polymers (CFRP) parts [5]. However, as reinforcing fibers, both carbon and glass, are sensitive with respect to tactile inspection, contact-free-measurement systems are advantageous in general [6].

Most studies concentrate on the formation of gaps or overlapping fibers during the process. Other common defects are twisting, wrinkling, foreign objects, as well as geometry and orientation changes [2], [4]. Studies show that gaps and overlaps result in a change of the mechanical properties of the laminate [7]–[10]: In general, gaps reduce the strength while overlaps may raise it locally, whereas potentially causing unwanted stress concentrations. Whereas many studies focus on the inspection of the final part surface or the laying process itself [4], [11], [12], this study demonstrates the use of a laser light sectioning sensor (LLSS) for inline geometry inspection of rovings. Glass fibers are difficult to measure due to their optical properties such as their transparency. Also, as stated in [3], the detection of both edges to determine a fiber's bandwidth can be limiting for laser-based measurements in certain conditions. For this purpose, a robust data processing strategy was developed, that adapts to various kinds of fiber and surface combinations as well as geometry alterations. In this work, an innovative method for processing the raw sensor data and for extracting the relevant fiber profile from the surface baseline is presented.

S. Neunkirchen and E. Fauster are with the Processing of Composites Group, Department Polymer Engineering and Science, Montanuniversität Leoben, 8700 Leoben, Austria (e-mail: stefan.neunkirchen@unileoben.ac.at).

By the time of her work S. Lehner was with the Christian Doppler Laboratory for Highly Efficient Composite Processing, Montanuniversität Leoben, 8700 Leoben, Austria.

P. O'Leary is with the Chair of Automation, Department Product Engineering, Montanuniversität Leoben, 8700 Leoben, Austria.

[1]Roving is a term in textile technology for a long, untwisted fiber bundle.

This article has been accepted for publication in IEEE Transactions on Instrumentation and Measurement. This is the author's version which has not been fully edited and content may change prior to final publication. Citation information: DOI 10.1109/TIM.2021.3132337

II. Process description and focus of this work

Filament winding specifies a family of processes for manufacturing of fiber-reinforced polymer composites. Depending on the type of incoming material, tape winding, wet winding and dry filament winding are distinguished in the composite processing community [13].

In this work, dry filament winding is addressed, where non-impregnated rovings are guided from spools to the winding mandrel, which rotates continuously. The winding pattern is realized by well-coordinated motions of the winding head (typically manipulated by a gantry platform or an anthropomorphic robot) relative to the winding mandrel, as shown in Fig. 1.

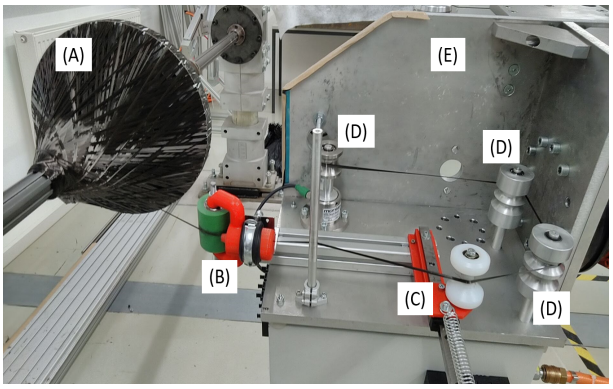

Fig. 1: Fiber guidance in a robotic filament winding head for the continuous winding of a conical structure with: winding mandrel (A), pull-out eye (B), tensioning unit (C), guiding rollers (D), and winding head (E).

The process allows the winding of a dry, fibrous preform, which is subsequently impregnated with a polymer matrix, which is finally cured (at elevated pressure and temperature, respectively) to result in the composite part.

Guiding of the rovings from the spool to the winding mandrel involves mechanical elements, such as rollers, deflection sheets and a pay-out eye/roller. When continuously guided, rovings tend to twist, compress or split. In worst case, breakage of individual, brittle filaments or significant portions of the roving can occur. Due to production inaccuracies of the raw material and the possible damaging of the rovings in the fiber guidance system, continuous inspection of the roving quality is required.

In order to scientifically study the impact of guiding elements as well as processing parameters on geometry and integrity of fiber bundles, a roving inspection test rig was designed as shown in Fig. 2. In this test rig, rovings are unwound from a fiber spool, redirected by a deflection roller, and guided through an inspection zone. Finally they are redirected again and wound up on a powered mandrel at a speed of $200°/s$. In the test rig, rovings of glass as well as carbon filaments will be studied, as these are the most widely used materials for reinforcing fibers. However, they exhibit vastly deviating optical properties: glass fibers are semi-transparent while carbon fibers are black in their raw design. For their application in fiber-reinforced polymer composites, they are typically conditioned by a so-called sizing,

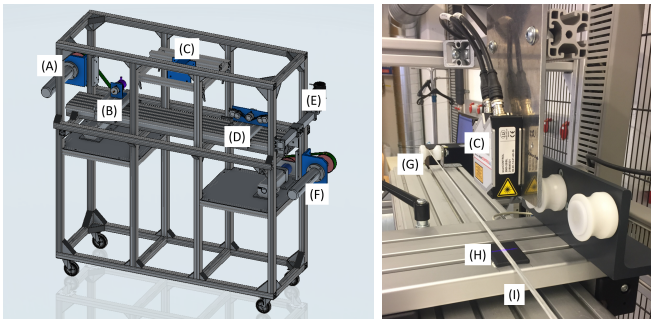

Fig. 2: Left: Roving inspection test rig used for studying geometric properties of rovings continuously transported under tensile load with: unwinding unit (A), rotary encoder (B), light sectioning sensor (C), tension load sensor (D), linear oscillating unit (E), and winding unit (F). Right: Experimental setup for the surface measurement, with: light sectioning sensor (C), guiding roller (G), black background plate (H), and glass roving (I).

which improves fiber-matrix adhesion in the final composite. Thus, the surface properties are particularly dependent of the type and distribution of the fiber sizing. As a result, optical properties of the rovings may vary from semi-transparent to non-transparent as well as from diffuse to specular reflective. In the present work, instrumentation of the roving inspection test rig and data analysis methods need to robustly cover this wide variety of optical properties. For the study at hand, a LLSS[2] was mounted on the roving inspection test rig. LLSS, also known as profile sensors, use the triangulation principle for two-dimensional profile detection. Using special optics, a laser beam is expanded into a static bright laser line and projected onto the surface of the object. A digital camera, located inside the sensor head, observes the diffusely reflected projection of the line on the object [14]–[18].

In composite processing, LLSS have been used for evaluating compaction [19] and spreading [20] of rovings. In both studies, the baseline was tilted and shifted to a horizontal level. Subsequently, the edges were detected by defining a threshold for the change in average height. Curved background conditions could not be described accurately and the definition of a threshold level for the edges was strongly dependent on human interaction. In [6], [21], [22] the measured data is used to implement an online path correction for an AFP-robot to minimize gaps in the placement process. These studies focus on the processing of the detected edges but give no further explanation of how the geometry of the tapes was determined mathematically.

The research focus of light sectioning in composite manufacturing processes up to this point lies in the interpretation and usage of the results gained by edge detection. A red laser light (wavelength >600 nm) was used in all the presented studies. A detailed description of the model to determine the exact position of the edges and thus the geometry is not given yet in literature.

[2] *scanCONTROL 2900-25/BL* by Micro-Epsilon Messtechnik GmbH.

This article has been accepted for publication in IEEE Transactions on Instrumentation and Measurement. This is the author's version which has not been fully edited and content may change prior to final publication. Citation information: DOI 10.1109/TIM.2021.3132337

Mack [23] used a laser micrometer to control the width of rovings with a spreading unit. This was necessary to ensure that the width is constant before an adhesive powder (so-called binder) could be applied uniformly. This is a potential use for the presented test rig. In this work four different backgrounds are analyzed on their usability for in-line measurement.

A. Experimental setup

The laser of the LLSS mounted to the roving inspection test rig creates a blue light at a wavelength of 405 nm. Blue laser light is chosen for the measurement of (semi-) transparent materials such as glass or PET [24] because it leads to a lower penetration depth and thus less diffusion. A very important factor in the measurement of surfaces with lasers are unwanted reflections, for example from a highly reflecting background like a polished metal. Therefore, a polished aluminum plate was chosen as background material to test the limits of the instrumentation. Additionally, a matte steel surrounding represents a very common background in machinery and tooling. As standard setup, a small black plate was attached right under the sensor, covering the area of the projected light beam, to prevent unsolicited reflections. Diametrically opposed to the black, also a thick white paper was used to illustrate the difference between the combinations of black and white fibers and surfaces respectively.
The LLSS was mounted on the roving inspection rig such that the sensor location is aligned with the major direction of the roving transportation and slight lateral motion of the roving can be captured [11]. The exposure time, the recorded time frame of one single profile, is one of the most important factors for the quality of the measurements. A high level of exposure time increases the intensity of light accumulated by the sensor and thus, the signal-to-noise ratio in the resulting data. However, due to the continuous motion of the roving with respect to the LLSS, high exposure time increases motion blur. By contrast, low exposure time may cause critically underexposed sensor readings. Thus, an optimizing trade-off had to be found.

Based on the previous experiments the following standard setup was defined:

1) Glass roving on a black background
2) Exposure time: $t_e = 5$ ms
3) Buffer: $n_p = 50$ profiles per second
4) Measurement period: $t_m = 20$ s

Consequently, $m = 1000$ profiles are acquired for each measurement and each profile consists of $n = 1280$ measurement points in the range $\pm 13\,mm$. Starting from this standard configuration further data were recorded to establish a broader database and to test the limits of the instrumentation. Glass fibers on a black background were tested with all possible exposure times from 0.001 to 40 ms (For 40 ms the buffered profiles per second needed to be adapted to 25 in order to get 1000 profiles). Other fiber and background materials were first started with the standard configuration. If the output data showed good results, the experiment was performed three times.

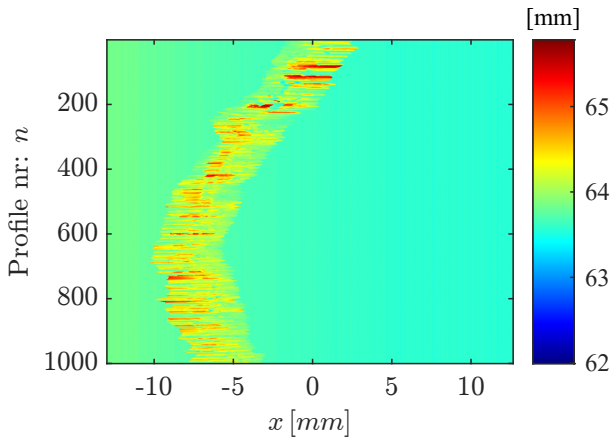

Fig. 3: Example of a complete set of raw data acquired by the instrumentation in the production equipment. It consists of $m = 1000$ cross section profile measurements, with a resolution of $n = 1280$ points in the range $\pm 13\,mm$. Note the background elevation varies systematically from left to right.

B. Data structuring

A necessary step to make further computational steps faster is to reduce the volume of the data. Due to the steady position of the sensor, the width of the projected line beam does not change during the measurement process. Therefore, it is sufficient to save only one set of data of the x-axes in the meta data.

The coordinates x_i, y_i and z_i of each point in the 3D space can be structured as: an $1 \times n$ row vector $\mathbf{x}$ with the locations where the elevations are measured; an $m \times 1$ time vector $\mathbf{t}$, in intervals of $t_r = 20$ ms, combined with the speed of the material yields the coordinate vector $\mathbf{y}$ and an $m \times n$ matrix $\boldsymbol{Z}$ containing the measured elevations. The matrix $\boldsymbol{Z}$ was stored in a table that associates each row with a certain time stamp.[3] The result of restructuring the data, is that every single profile can now be easily extracted from the data table.

III. Data processing

The task now is to extract the required information from the raw data. An example of a complete measurement is shown in Figure 3. The data in this manner can be regarded as a matrix $\boldsymbol{Z}$ of elevations, with a vector $\mathbf{x}$ containing $n = 1280$ x-locations in millimeters and the vector $\mathbf{y}$ corresponding to the measurement numbers. Handling the data as a matrix simplifies the application of algebraic techniques for tensor approximations.

Now considering this exemplary data we can define the information we wish to extract from this raw data:

1) The background level in the data varies systematically from left to right. The range of this variation 2–3 *mm* is due to misalignment of the measurement head wrt. to the background plane. It is small; however, removing it simplifies the proceeding computations.

[3]In Matlab this is referred to as *timetable*, in Python it is called a *Panda dataframe*.

This article has been accepted for publication in IEEE Transactions on Instrumentation and Measurement. This is the author's version which has not been fully edited and content may change prior to final publication. Citation information: DOI 10.1109/TIM.2021.3132337

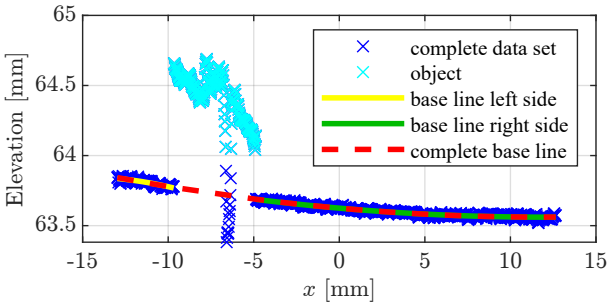

Fig. 4: Example of a profile measured during the real time measurement of the roving.

2) The roving, which should be a straight band, is moving laterally during production; partially due to the process of unwinding from a spool. It is desirable to know the instantaneous position of the center line of the roving, since this is relevant for the positioning on the element being produced.
3) There are strong variations in the measured elevation of the roving. There are multiple effects at work here; vibrations of the roving change its elevation and this is accentuated by the changing optical conditions when the angles between the roving and the laser plane of light are continually changing.
4) There are also changes in the width of the roving which need to be characterized. This is due to the roving be strands of material that change their relative positions under tension. Under some circumstances, this actually leads to a gap in the roving, see for example the profile measurement presented in Figure 4. Here, only the points marked in light blue are treated as parts of the object: Small gaps caused by friction effects should not be considered for the geometry calculations.

A. Individual Baseline compensation

An example of a single measurement profile is shown in Figure 4. The systematic variation of the baseline can be seen from the left to the right. The goal here is to model this background and compensate for it in the data.

Base line compensation is a task also encountered in spectral analysis [25], [26]; however, the base line compensation required here is much simpler. The baseline is based on a least squares polynomial approximation with the detection and segmentation based on outliers [27] for each profile; followed by a tensor polynomial approximation [28] to reduce the effects of noise. The advantage of this approach lies in the wide fields of application, because ultimately the model fitting method is not limited by certain surfaces or shapes; furthermore, it has a low susceptibility to noise.

The challenge here is to determine which data points belong to the baseline and which to the object, independently of the amount of reflections and of the geometric characteristics of the object, such as spreading or splitting. In [26], the authors propose a measure, Equation 1 in their work, for the optimization process based on the integral over the absolute values of the data and a baseline model. This choice is driven by the fact that there may never be negative spectral components and the power integral is relevant. However, the optical properties of the materials being inspected here can lead to apparent negative values which need to be determined.

Here an iterative polynomial approximation has been chosen to obtain the model for the baseline. The baseline $\mathbf{z}_b$ is modelled as a polynomial in x with the coefficient vector α, i.e., $\mathbf{z}_b = \mathsf{p}(\alpha, x)$.

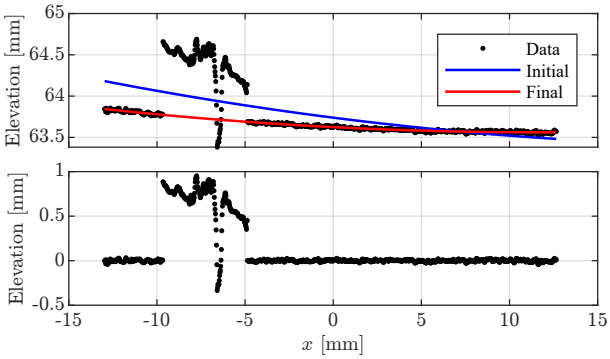

Fig. 5: Top: Example of a single base line computation, for the data shown in Figure 4. The raw data, the initial approximation and the final converged result are shown above. Below: the data after base line compensation.

The algorithm proceeds in the following steps, for all $k \in [1 \ldots m]$ measurements:

Step 1: Given the row vectors $\mathbf{x}_k$ and $\mathbf{z}_k$ for the k^{th} measurement, the background profile is initialized as $\mathbf{x}_b = \mathbf{x}_k$, $\mathbf{z}_b = \mathbf{z}_k$, i.e., it starts with the complete data.

Step 2: Compute the Vandermonde matrix $\boldsymbol{V}(\mathbf{x_b})$ for the x-locations $\mathbf{x}_b$, denoted as $\boldsymbol{V}$ for simplicity.

$$\mathbf{z}_b = \boldsymbol{V}\,\alpha. \tag{1}$$

The inverse of $\boldsymbol{V}$ is computed using QR decomposition to ensure both numerical stability and efficiency, i.e., given $\boldsymbol{V} = \boldsymbol{Q}\,\boldsymbol{R}$, then,

$$\alpha = \boldsymbol{R}^{-1}\,\boldsymbol{Q}^{\mathrm{T}}\,\mathbf{z}_b. \tag{2}$$

Since this is a linear process the covariance of the coefficients $\boldsymbol{\Lambda}_\alpha$ can be computed [29] as,

$$\boldsymbol{\Lambda}_\alpha = \boldsymbol{R}^{-1}\,\boldsymbol{Q}^{\mathrm{T}}\,\boldsymbol{\Lambda}_{z_b}\,\boldsymbol{Q}\,\boldsymbol{R}^{-1^{\mathrm{T}}}. \tag{3}$$

If we assume that in the converged state the residual is Gaussian, as is the case here, then $\boldsymbol{\Lambda}_{z_b} = \sigma_z^2\,\boldsymbol{I}$, with σ_z being the standard deviation; further more, $\boldsymbol{Q}^{\mathrm{T}}\,\boldsymbol{Q} = \boldsymbol{I}$ we obtain the simplified equation,

$$\boldsymbol{\Lambda}_\alpha = \sigma_z^2\,\boldsymbol{R}^{-1}\,\boldsymbol{R}^{-1^{\mathrm{T}}}. \tag{4}$$

With this, both the coefficients and their covariance are known.

Step 3: Evaluate the residual vector $\mathbf{r} = \mathbf{z}_b - \boldsymbol{V}\,\alpha$ and the prediction uncertainty $\varepsilon = f\,\mathrm{diag}\left\{\boldsymbol{V}\,\boldsymbol{\Lambda}_\alpha \boldsymbol{V}^{\mathrm{T}}\right\}$ for each point; f is selected to obtain the desired level of prediction, here $f = 5$. In the case of Gaussian perturbations the confidence level $c = 99.99$ corresponds to 4σ. For non-Gaussian data the Chebyshev inequality can be used to obtain a lower bound on

This article has been accepted for publication in IEEE Transactions on Instrumentation and Measurement. This is the author's version which has not been fully edited and content may change prior to final publication. Citation information: DOI 10.1109/TIM.2021.3132337

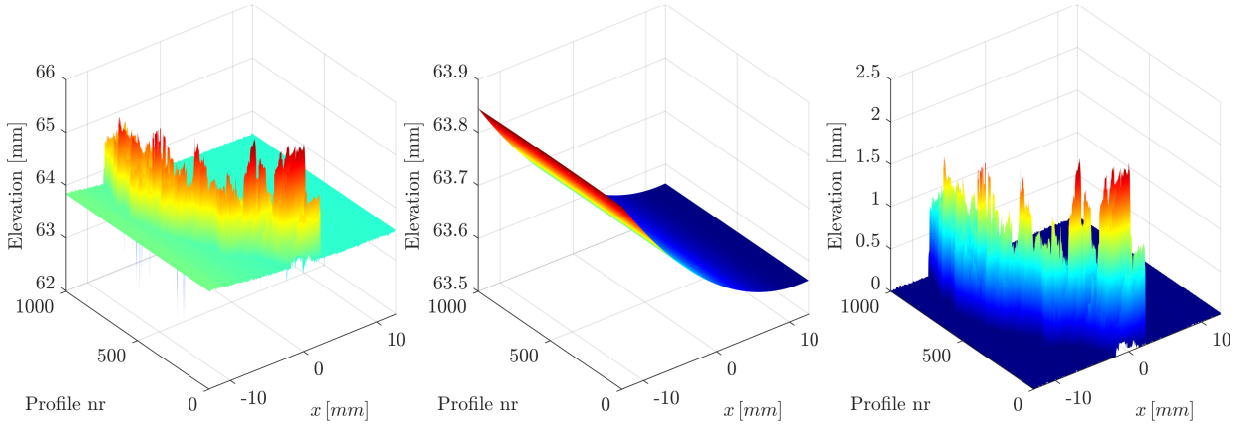

Fig. 6: Left: Raw data for a complete measurement prior to base line compensation. Center: Tensor polynomial approximation for the base values. Right: Data after base level compensation.

the certainty c_1, in this case a value of c_1=94%. This level is used to segment the active portion of the profile from the base line.

Step 4: Identify the indices $\mathbf{i}$ for the points where $\mathbf{r}(\mathbf{i}) \leq \varepsilon(\mathbf{i})$, i.e., the points within the desired degree of certainty. Then select these points for further processing, $\mathbf{x}_b = \mathbf{x}_b(\mathbf{i})$ and $\mathbf{z}_b = \mathbf{z}_b(\mathbf{i})$.

Step 5: Test if the residual vector $\mathbf{r}$ is Gaussian, e.g. are the inter-quantile range (IQR) and the 50% confidence interval of $\mathbf{r}$ consistent with a Gaussian probability function. For this, a Kolmogorov–Smirnov test can also be used. If the test succeeds, the final result is found and the iteration process can be stopped. Otherwise, repeat from **Step 2**. This algorithm has proved successful and efficient for all profiles, it typically converges after $p = 4$ iterations. An example profile, the initial polynomial approximation and the final converged base line are shown in Fig. 5, together with the corrected data.

B. Complete baseline compensation

The individual baselines are subject to perturbations due to noise in the raw data. A further improvement in the base compensation can be obtained by applying a tensor polynomial approximation to all the baseline data. This is a simple task since all the data for $\boldsymbol{Z}_b$ now lie on a regular lattice and the approximations in the x direction are already performed. Consequently, it is now only necessary to perform the second portion of the tensor approximation, i.e., in the y direction. This is achieved as follows, compute a Vandermonde $\boldsymbol{V}_y$ matrix, of the desired degree d, for the y direction. The tensor approximation $\boldsymbol{Z}_t$ for the complete background is calculated as,

$$\boldsymbol{Z}_t = \boldsymbol{V}_y \left(\boldsymbol{V}_y^{+} \boldsymbol{Z}_b \right), \tag{5}$$

whereby, the brackets indicate the sequence of computation to ensure numerical efficiency. Finally, the baseline compensated data matrix $\boldsymbol{Z}_c$ is computed,

$$\boldsymbol{Z}_c = \boldsymbol{Z} - \boldsymbol{Z}_t. \tag{6}$$

An example data set with the tensor polynomial surface for the baseline compensation and the resulting corrected data is shown in Figure 6. This yields a baseline compensation for the complete data set that is significantly more stable than the methods originally presented in [1].

C. Data alignment and center line detection

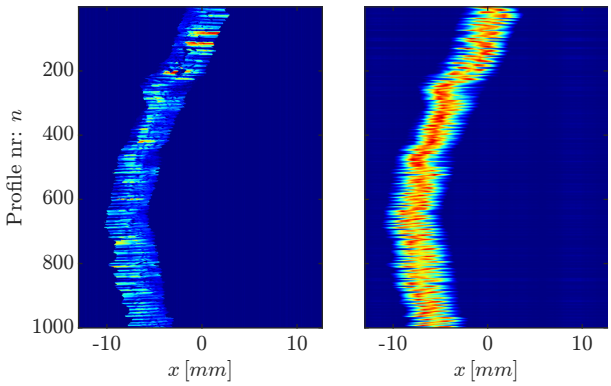

Fig. 7: Left: baseline corrected data. Right: the same data after normalization.

There are a number of issues which need to be detected during the winding process, e.g. roving compaction, spreading, splitting or filament breakage, since these have negative consequences for the manufactured parts. The goal now is to align the individual profiles so as to obtain a straight representation of the roving; this also yields a trajectory for the center of the roving. As can be seen in Figure 3, there is a significant variation of the elevation and position of each measured profile. The past solution [1] was to simply segment the data based on a level derived from the approximation uncertainty level. However, this approach can be sensitive to low elevation observed in some profiles. Consequently, a new approach has been developed, which proceeds as follows:

Step 1: Each row of the matrix $\boldsymbol{Z}_c$ is normalized by its respective 2-norm, to obtain $\boldsymbol{Z}_n$. This standardizes the magnitude of

This article has been accepted for publication in IEEE Transactions on Instrumentation and Measurement. This is the author's version which has not been fully edited and content may change prior to final publication. Citation information: DOI 10.1109/TIM.2021.3132337

the data as a whole without modifying its inner structure. The result of this process is shown in Fig. 7.

Step 2: The cross correlation of each normalized profile is computed wrt. a reference profile; here the mean of a number of starting profiles are used, since the roving is always started in an appropriate position. The locations of the maximum correlations, in each row, yields a vector $\mathbf{x}_{cl}$, of estimates for the locations of the center line as a function of time. An example for the correlations and locations can be seen in Fig. 8. The advantage of correlation is that it uses all the data

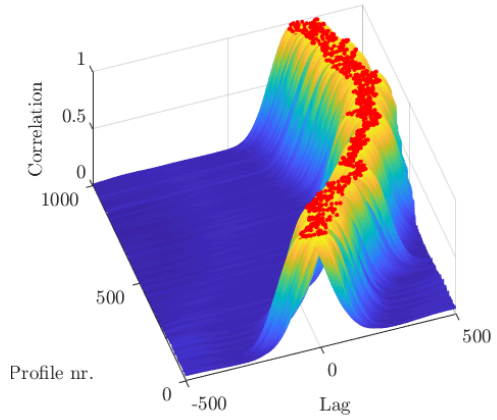

Fig. 8: Center line of the roving as a function of time.

points and random Gaussian noise will have no correlation, except at zero shift. This yields a very stable estimate for the roving center line, see Fig. 9. As stated in [21], path correction, and therefore reducing gaps during the winding process, increases the quality of the finished product.

Step 3: The center line estimates are used to realign the individual profiles, the result of this is shown in Fig. 10.

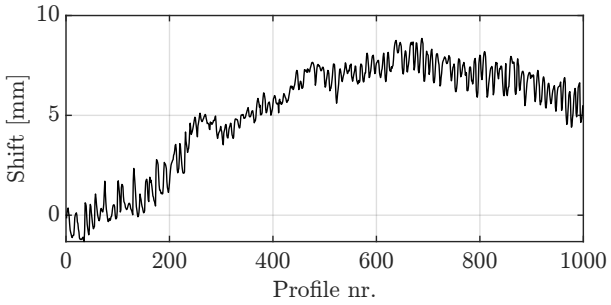

Fig. 9: Estimate for the center line of the roving as a function of time, as obtained from the correlation analysis.

The results for a second measurement are shown in Fig 11; note: this data set contains abrupt snapping in position of the rowing, possibly due to tension. The algorithm has correctly detected and compensated for this.

D. Roving width

The edges of the roving also permit to measure the width of the roving as a function of time, see Fig. 12. The tendency of a roving to get split, spread, or compacted can be seen directly

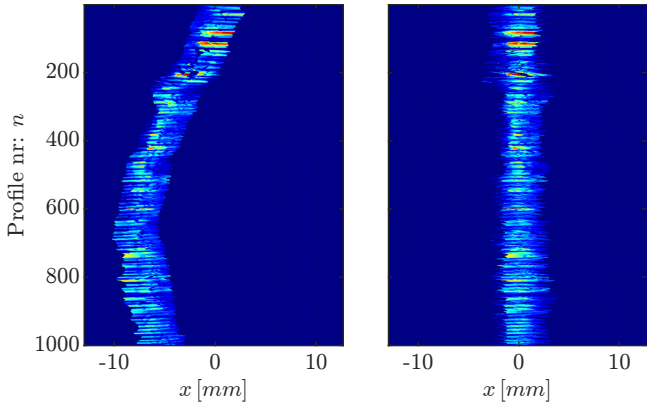

Fig. 10: Left: Baseline corrected data. Right: data after applying the alignment algorithm.

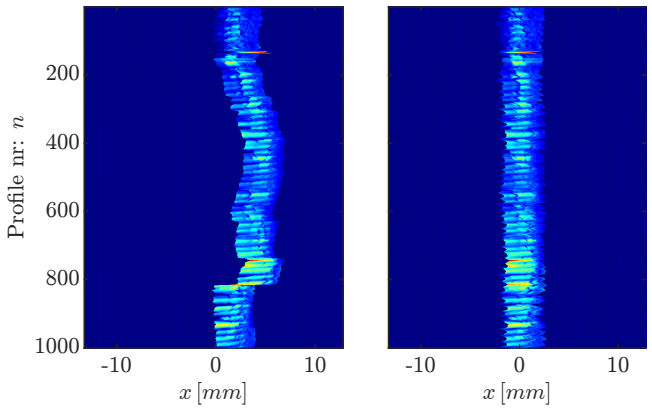

Fig. 11: Left: Baseline corrected data. Right: data after applying the alignment algorithm. Note: this data set contains abrupt steps in the position of the roving, resulting from the snapping in position due to tension.

in the width measurement. An increasing width correlates with the spreading of the roving, and a shrinking width goes hand in hand with the compacting of the roving. It can clearly be seen, that the width of the roving fluctuates during the winding process. When comparing the width of each profile with the center line location in Fig. 9, some correlation can be observed. At profile number ∼220, a maximum in width and a 'buckle' of the center line can be seen. This can be explained by a spreading of the roving due to surface friction. On a smaller level, the same can be observed at profile number ∼450. The detection of the width during the winding process makes it possible to do further path correction.

E. Splitting of the rowing

With the quality of the baseline compensation it is now a simple task to detect splitting of the roving; an example case is shown in Fig. 13. This roving has split into two strands, which is a highly undesirable during production process.

IV. Roving tension and oscillations

The original goal has been achieved above. However, the availability of the aligned data permits the computation of

This article has been accepted for publication in IEEE Transactions on Instrumentation and Measurement. This is the author's version which has not been fully edited and content may change prior to final publication. Citation information: DOI 10.1109/TIM.2021.3132337

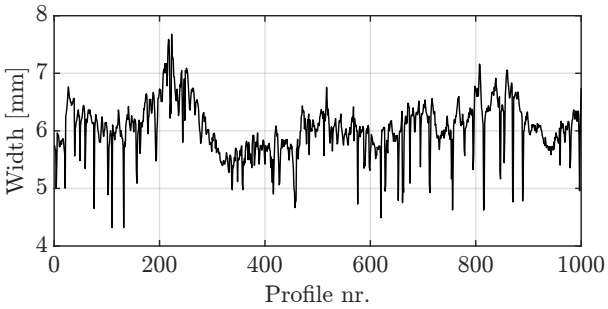

Fig. 12: Width of the roving; note, systematic changes in the width as a function of time can be observed.

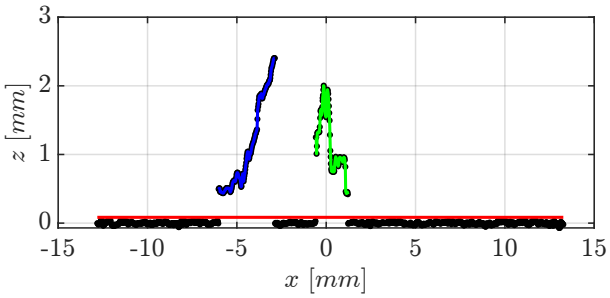

Fig. 13: Application of the corrected baseline on the example of a manually split roving. The two partitioned object segments are marked in green and blue, the corrected baseline is marked in red.

additional properties. It is of particular interest to characterize the oscillations and spatial changes in tension on the roving.

A. Global oscillations

An FFT can be applied to the data across all x locations to obtain a characterization of the oscillation frequencies as a whole, see Fig. 14. Here, a clear tendency of the roving to vibrate at $0.1\,f_m = 5\,\text{Hz}$, where f_m is the measurement frequency, is seen.

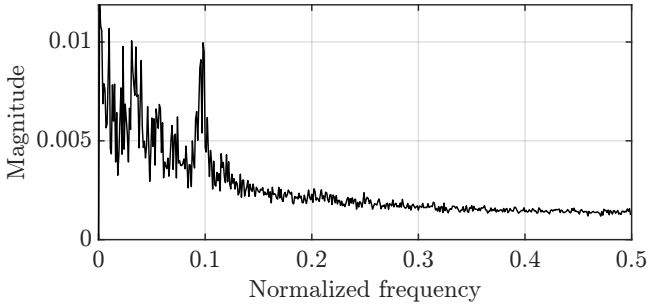

Fig. 14: Discrete Fourier analysis across x. Noticeable peak at $0.1\,f_m = 5\,\text{Hz}$.

B. Spatial oscillations and tension

Alternatively, it is possible to compute the spectrum for each x location, to obtain information of the spatial distributions of oscillations across the roving. An example is shown in Fig 15. In this example there is a stronger tendency of the roving to oscillate near the center. A second example on a roving of a different size and its spatial vibrations is shown in Fig. 16. In this example the roving tends to vibrate more strongly on the right hand side at approx $f_o = 2.6\,\text{Hz}$. This would indicate a variation in tension across the roving, an issue that should be addressed in a production process.

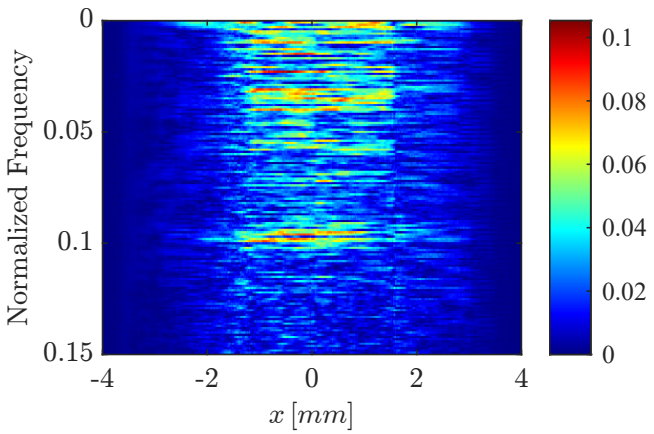

Fig. 15: Fourier spectrum for each vertical track. Note: in this figure the frequencies are relative to the measurement frequency f_m.

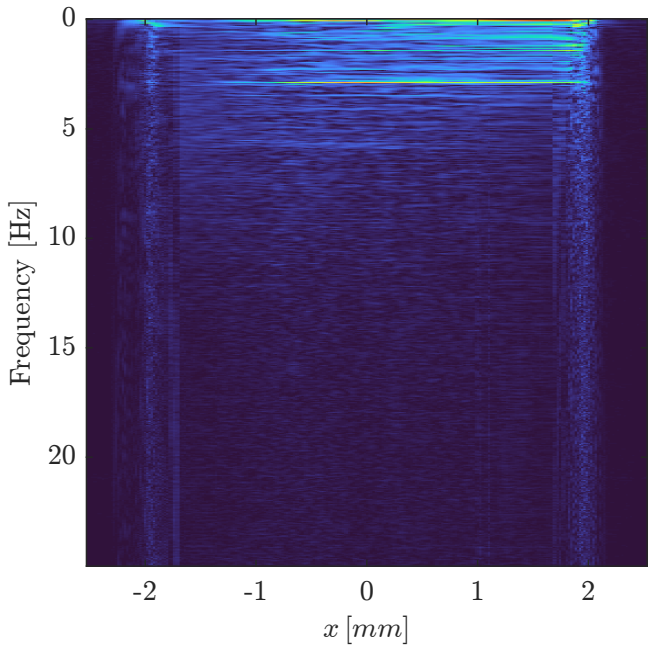

Fig. 16: Fourier spectrum for each vertical track. Note: in this example the roving tends to vibrate more strongly on the right hand side at approx $f_o = 2.6\,\text{Hz}$.

V. Results & Discussion

The aim of this work was to develop a reliable, robust, and universally usable algorithm for the in-line monitoring of rovings but also to investigate the limits of the instrumentation. While the code proved to deliver good results for any given

data set, it often failed to create such a set of processable data. In the experimental setup, no effort was put into the improvement of the data recording since the test conditions should be close to the later industrial application. For example, the roving was not pressed onto the surface in the measurement area and its movement was strongly influenced by (unintentional but very common) forces from the spool's unwinding at the edges and from the braking system.

A. Glass

Glass rovings were tested in the full range of the sensor's exposure time. As expected, the detection of glass fibers works on any background within the range of exposure times from 5–20 ms.

B. Carbon

Two types were tested: 'regular' rovings and rovings treated with a powder binder material. Binder is applied to the roving at high temperatures and provides better adhesive properties when used in a heated dry winding process. In consequence, these binder rovings are more 'tape-like' and have a rather well-defined geometry. While the detection of regular carbon fibers on any surface failed, the bindered rovings could be recognized by the sensor with an exposure time of 5 ms. It is assumed that the loose filaments in the carbon fiber roving lead to specular reflection which can not be detected by the sensor camera. In these data sets, only the absence of light in the place of the roving could be tracked. Bindered rovings (with the same amount of filaments) on the other hand form a much tighter bond and have also an almost grey surface due to the remaining binder powder particles. An optimized housing of the measurement area could enable the sensor to detect the profile of carbon fibers reliably. A nearly perfect black background or surface modifications on the rovings are possible options. Considering bindered rovings the given instrumentation can be sufficient but it has to be ensured that lighting and background conditions are optimized.

VI. Summary & Conclusion

A robust method to process geometric measurement data of rovings with a light sectioning sensor was presented. Cross-correlation enables the evaluation of the roving geometry and lateral movement. The center line and the roving width can be determined reliably as important input parameters for process control. Detection of defects such as splits as well as abnormalities in lateral oscillation can help to identify errors in the raw material or the process setup.

The given instrumentation was evaluated for various fiber types and backgrounds. While glass fibers are relatively easy to monitor with an LLSS, the detection of carbon fiber needs improvement in the instrumentation and the treatment of the fibers. Surface properties of (topically treated) carbon fibers have to be examined in order to determine the measurement range of the respective sensors. Finally, background and lighting conditions need to be evaluated to facilitate proper data acquisition. The findings presented in this paper can be used to implement in-line monitoring for the support of automated process control. As the next step, this adaption needs to be addressed. Data recording and subsequent real-time processing must be automated. Challenges of a production environment, compared to the test rig in this work, must be considered in terms of pollution, vibrations, background conditions, and other influences on the measurement process. This will provide a significant contribution to the process surveillance in the processing of continuous fibrous reinforcements.

Acknowledgment

The authors kindly thank the Bundesministerium fuer Digitalisierung und Wirtschaftsstandort and the FACC Operations GmbH for their funding of this research as well as the Christian Doppler Forschungsgesellschaft for their administrative support.

References

[1] S. Lehner, S. Neunkirchen, E. Fauster, and P. O'Leary, "Instrumentation of a roving inspection test rig with surface geometry measurement of fiber bundles," in *IEEE 2021 Int. Instrumentation and Measurement Technology Conf. (I2MTC)*, pp. 1–6.

[2] K. Schlegel, "A literature review of quality control for automated lay-up processes," *J. Plast. Technol.*, vol. 1, pp. 392–436, 2019.

[3] C. Hopmann, N. Magura, N. Rozo Lopez, D. Schneider, and K. Fischer, "Detection and evaluation of the fibers' deposition parameters during wet filament winding," *Polym. Eng. Sci.*, vol. 61, no. 5, pp. 1353–1367, 2021.

[4] F. Shadmehri, O. Ioachim, O. Pahud, J.-E. Brunel, A. Landry, S. V. Hoa, and M. Hojjati, "Laser-vision inspection system for automated fiber placement (AFP) process," in *ICCM20*, Copenhagen, Denmark, Jul.2015.

[5] E. Oromiehie, B. G. Prusty, P. Compston, and G. Rajan, "Automated fibre placement based composite structures: Review on the defects, impacts and inspections techniques," *Compos. Struct.*, vol. 224, p. 110987, 2019.

[6] C. Krombholz, M. Bock, M. Perner, D. Röstermundet, and M. Meyer, "Online Bahnkorrektur eines Industrieroboters mittels optischer Sensoren für den Einsatz im Fiber–Placement–Prozess," in *60. Deutscher Luft- und Raumfahrtkongress*. Bonn, Germany: Deutsche Gesellschaft f. Luft- u. Raumfahrt, 2011, pp. 503–513.

[7] K. Croft, L. Lessard, D. Pasini, M. Hojjati, J. Chen, and A. Yousefpour, "Experimental study of the effect of automated fiber placement induced defects on performance of composite laminates," *Compos. Part A: Appl. Sci. and Manuf.*, vol. 42, no. 5, pp. 484–491, 2011.

[8] M. Lan, D. Cartié, P. Davies, and C. Baley, "Influence of embedded gap and overlap fiber placement defects on the microstructure and shear and compression properties of carbon–epoxy laminates," *Compos. Part A: Appl. Sci. and Manuf.*, vol. 82, pp. 198–207, 2016.

[9] M. Belhaj, M. Deleglise, S. Comas-Cardona, H. Demouveau, C. Binetruy, C. Duval, and P. Figueiredo, "Dry fiber automated placement of carbon fibrous preforms," *Compos. Part B: Eng.*, vol. 50, pp. 107–111, 2013.

[10] M. H. Nguyen, A. A. Vijayachandran, P. Davidson, D. Call, D. Lee, and A. M. Waas, "Effect of automated fiber placement (AFP) manufacturing signature on mechanical performance of composite structures," *Compos. Struct.*, vol. 228, p. 111335, 2019.

[11] R. Schmitt, C. Niggemann, and C. Mersmann, "Contour scanning of textile preforms using a light-section sensor for the automated manufacturing of fibre-reinforced plastics," in *Opt. Sensors 2008*, ser. SPIE Proceedings, F. Berghmans, A. G. Mignani, A. Cutolo, P. P. Meyrueis, and T. P. Pearsall, Eds. SPIE, 2008, p. 70031I.

[12] ——, "Laser light-section sensor automating the production of textile-reinforced composites," in *Opt. Sensors 2009*, ser. SPIE Proceedings, F. Baldini, J. Homola, and R. A. Lieberman, Eds. SPIE, 2009, p. 73560P.

[13] T. Sofi, S. Neunkirchen, and R. Schledjewski, "Path calculation, technology and opportunities in dry fiber winding: a review," *Adv. Manuf.: Polym. & Compos. Sci.*, vol. 4, no. 3, pp. 57–72, 2018.

[14] scan CONTROL, "product catalog," Micro-Epsilon GmbH, Accessed: May 2, 2020. [Online]. Available: https://www.micro-epsilon.de/download/products/cat--scanCONTROL--de.pdf
[15] E. Fauster, "Calibration method for light sectioning measurement systems," in *2nd WSEAS Int. Conf. Signal, Speech and Image Process.*, Skiathos, Greece, Sep. 2002.
[16] L. Traxler, L. Ginner, S. Breuss, and B. Blaschitz, "Experimental comparison of optical inline 3d measurement and inspection systems," *IEEE Access*, vol. 9, pp. 53 952–53 963, 2021.
[17] P. O'Leary, P. Schalk, R. Ofner, and A. Gfrerrer, "Instrumentation and analysis-methods for the measurement of profiles using light sectioning," in *IEEE 2006 Instrumentation and Measurement Technology Conf. Proc.*, Sorrento, Italy, pp. 1108–1113.
[18] P. Schalk, P. O'Leary, R. Ofner, and A. Gfrerrer, "Measuring and analyzing cross-sectional profiles of rotating objects using light sectioning," *IEEE Trans. Instrum. Meas.*, vol. 57, no. 10, pp. 2329–2338, Oct. 2008.
[19] D. Kastanis, H. Steiner, E. Fauster, and R. Schledjewski, "Compaction behavior of continuous carbon fiber tows: an experimental analysis," *Adv. Manuf.: Polym. & Compos. Sci.*, vol. 1, no. 3, pp. 169–174, 2015.
[20] M. Tonejc, H. Steiner, E. Fauster, S. Konstantopoulos, and R. Schledjewski, "A study on geometrical parameters influencing the mechanical spreading of fibre bundles," in *ICCM20*, Copenhagen, Denmark, Jul. 2015.
[21] C. Krombholz, M. Perner, M. Bock, and D. Röstermundet, "Improving the production quality of the automated fiber placement process by means of online path correction," in *28th Int. Congr. Aeronaut. Sci.*, Brisbane, Australia, Sep. 2012.
[22] C. Nguyen, C. Krombholz, and D. Röstermundet, "Einfluss einer Online Bahnkorrektur auf die Materialeigenschaften von Prepreg Tows im Fiber Placement Prozess," in *Deutscher Luft- und Raumfahrtkongress*, Berlin, Germany, Sep. 2012.
[23] J. Mack, *Entwicklung eines adaptiven Online-Bebinderungsprozesses für die Preformherstellung: Zugl.: Kaiserslautern, Techn. Univ., Diss., 2015*, ser. IVW-Schriftenreihe. Kaiserslautern: Inst. für Verbundwerkstoffe, 2015, vol. 115.
[24] A. V. Mel'nik, A. V. Seredkin, M. P. Tokarev, and O. A. Gobyzov, "Laser line scanning of a shape of moving objects with various degree of transparency," *J. Phys.: Conf. Ser.*, vol. 1677, p. 012187, 2020.
[25] C. B. Nelson, "Least squares gamma spectrum analysis with automatic gain and baseline compensation," *IEEE Trans. Nucl. Sci.*, vol. 17, no. 1, pp. 428–435, 1970.
[26] D. Barkauskas and D. Rocke, "A general-purpose baseline estimation algorithm for spectroscopic data." *Anal. Chim. Acta*, vol. 657, no. 2, pp. 191–197, 2010.
[27] F. Bookstein, "Fitting conic sections to scattered data," *Comput. Graph. and Image Process.*, vol. 9, no. 1, pp. 56–71, 1979.
[28] T. Ma, J. Shi, and D. Steurer, "Polynomial-time tensor decompositions with sum-of-squares," in *2016 IEEE 57th Annu. Symp. Foundations of Computer Science (FOCS)*, 2016, pp. 438–446.
[29] K. M. Ramachandran and C. P. Tsokos, *Mathematical statistics with applications in R*, 2nd ed. London, UK: Academic, 2015.

Stefan Neunkirchen received a diploma in mechanical engineering from TU Kaiserslautern, Germany in 2016 and is now working as a PhD student with the Processing of Composites Group at the Montanuniversität Leoben. His research interest is the process development and automation of composite manufacturing processes. In particular, he is working on the robotic, dry filament winding process.

Ewald Fauster Ewald Fauster joined the newly founded Processing of Composites Group at Montanuniversität Leoben, Austria, in 2011. He completed his habilitation in 2018, for which he was appointed as an associate professor at Montanuniversität Leoben. His major fields of research cover the automated processing of fiber-reinforced polymer composites as well as measurement technology, in particular optical techniques with digital image processing.

Sophia Lehner is currently a master's student at the Chair of Automation at the Montanuniversität Leoben. In frame of her thesis she performed experiments on the instrumentation and data evaluation of a light sectioning sensor on a roving test rig and presented them at the I2MTC 2021.

Paul O'Leary is Professor for Automation at the University of Leoben. His research focuses on mathematical methods to extract information, knowledge and understanding from data. He has degrees in Mathematics and Engineering from Trinity College Dublin, Ireland; a M.Sc. in Electronics Engineering of PII Eindhoven, Netherlands and a PhD from the University of Pavia, Italy.